

Non-deterministic dynamics of a mechanical system

Robert Szalai & Mike R. Jeffrey

Engineering Mathematics, University of Bristol, UK, email: r.szalai@bristol.ac.uk

(Dated: February 17, 2014)

A mechanical system is presented exhibiting a non-deterministic singularity, that is, a point in an otherwise deterministic system where forward time trajectories become non-unique. A Coulomb friction force applies linear and angular forces to a wheel mounted on a turntable. In certain configurations the friction force is not uniquely determined. When the dynamics evolves past the singularity and the mechanism slips, the future state becomes uncertain up to a set of possible values. For certain parameters the system repeatedly returns to the singularity, giving recurrent yet unpredictable behaviour that constitutes non-deterministic chaotic dynamics. The robustness of the phenomenon is such that we expect it to persist with more sophisticated friction models, manifesting as extreme sensitivity to initial conditions, and complex global dynamics attributable to a local loss of determinism in the limit of discontinuous friction.

I. INTRODUCTION

Classical mechanics accounts for motion of both rigid and deformable bodies, describing macroscopic processes, often with great accuracy. Even for simple bodies, however, the contact forces between them can be particularly complex, and one must resort either to intricate fine scale models or crude empirical approximations. This is the case for both friction and impact. In impact, reaction forces vary by several magnitudes within the very short time interval that contact occurs. Models are generally empirical, taking the form of kinematic constraints given between infinitesimally close times where contact is made and lost [4, 28, 29]. Friction, on the other hand, describes a resistance force between surfaces in sustained contact. The evolution of the friction force over significant time intervals stands as a singularly enduring problem in classical rigid body mechanics, as a brief inspection of the extensive literature reveals. Common empirical force laws still largely resemble those set down by Da Vinci, Amontons and Coulomb (see e.g. [4, 10, 23, 32]), of a constant force opposing the direction of motion. This simplicity is in contrast with experimental images that reveal a complex evolution of the contact surface [2, 3, 20, 22, 25].

The difficulties in obtaining a clear theory of friction are further complicated by the coefficient of friction varying with scale, material, motion, and physical conditions such as temperature and lubrication. Theorists and experimentalists continue to seek improved contact models by allowing,

for example, impact compliance [5, 13], frictional memory [12, 27], speed dependence (Stribeck effect) [20, 32], and microscopic structure such as asperity deformation at the frictional interface [1, 2].

Regardless of the chosen model, mechanical laws are reasonably associated with deterministic dynamics. Reliable models are vital in the study of tyre deformation in the automotive and aeronautic industries, of drill strings, turbine rotors, and so on. To this end, all of the contact models discussed above tend to retain one essential feature of friction and impact, and that is discontinuity, either from switching between free-flight and in-contact impact laws, or switching between “left-motion” and “right-motion” friction laws. It is easy to assume that one may smooth out the discontinuity. The effects of smoothing on the dynamics, however, remain poorly understood, with both theory and simulations suggesting more intricate dynamics organised, nevertheless, around the quantitative features of the discontinuous limit [15].

The crucial point is that existence and uniqueness of the dynamical solutions of differential equations is not guaranteed when they suffer discontinuities. In many situations, including all those listed above, the existence of solutions can be guaranteed at the possible expense of loss of uniqueness. The most obvious example is a slipping block that comes to rest on a surface. It is easy to predict where the block will stop, but when it comes to rest information about its previous motion is lost to the environment, and piecing together its previous motion is no longer possible. This loss of unique reversibility is common in a piecewise-smooth dynamical system. When a trajectory encounters a discontinuity there are local rules, physically motivated, that provide a well-defined and solvable system. But those solutions may be non-unique either in forward or backward time. Backward time ambiguity corresponds to the onset of sticking that brings a block to rest, consistent with centuries of physical intuition. Forward time ambiguity, on the other hand, signals a breakdown in the deterministic character of physical law.

A classic example of a forward time ambiguity is the Painlevé paradox (see e.g. [5]) responsible for the juddering of a piece of chalk when pushed, instead of dragged, along a blackboard. As a rod impacts a surface its endpoint can stick in place or slip. The effects of impact and friction, together with the coupling of the rod’s linear and angular motion, may combine such that the surface seems to attract, rather than resist, the rod. The rod’s release is then not uniquely determined by the governing equations, resulting in unpredictable skipping of its endpoint along the surface. In this paper we present a phenomenon that is potentially more common, and more extreme, where forward and backward time ambiguity combine to generate chaotic dynamics.

This behavior was described in a theoretical context in [7], and in an abstract model proposed

in [14]. The discontinuity in a piecewise-smooth system can create a so-called two-fold singularity, where a system switches between two states, which both evolve instantaneously along the switching locus. Two-fold singularities arise in generic systems of more than two dimensions (with simpler degenerate forms in planar systems). They have different forms, some of which are benign, either in the sense that they are invisible to the dynamics, or that forward time ambiguities are short-lived because trajectories quickly recombine. In another form, trajectories enter the singularity both forwards and backwards in time, traveling (counterintuitively) from attracting regions to repelling regions of phase space, and in a finite amount of time. The result is a set of allowed future and past trajectories, with none more likely than any other. In [7], local conditions near a bifurcation were shown to re-inject trajectories so that this unpredictable singularity was visited repeatedly, giving birth to a non-deterministic form of chaos. In [14], a global re-injection mechanism was shown to create more robust non-deterministic chaos in an abstract system with negative damping. Attempts have also been made to characterize the possible appearance of the singularity in electrical control models [6, 9].

Despite these steps, no testable examples of this singular prediction of piecewise-smooth dynamical systems theory have previously been devised. In this paper the singularity is shown to occur in a simple and realistic mechanical model, motivated from devices such as [31], involving a Coulomb friction law and a simplified version of Pacejka's magic formula [24] to characterize nonlinear response of a wheel. Non-deterministic chaos ensues for a range of parameters, and while a continuum model such as the stretched string tyre model [30] should resolve the singularity, the sensitivity to initial conditions that gives rise to chaos-like dynamics is expected to persist.

Below we present the mechanical model in section II, and show how a singularity arises in the friction force in section III. Some generalities of the singularity are presented briefly in section IV, followed by identification of parameter regimes for which non-deterministic chaos can appear along with simulations in section V. We remark on special simplifying cases in VI and make concluding remarks in section VII.

II. MECHANICAL MODEL

The crucial component of the following mechanical system is the friction torque and the friction force imparting on a wheel that can balance each other with respect to the constraints built into the system. The precise design of the mounting of the wheel on a rotating disc is contrived solely to simplify the analysis by eliminating the rotation angle of the mount from the equations of motion.

Figure 1 shows the mechanical model of interest. It consists of two discs that can independently rotate on a shared axis, and a wheel (shown red) mounted transversely inside the upper disc so that it rolls over the surface of the lower disc. The wheel is mounted inside the top disc by means of a slider (a one degree of freedom oscillator, shown in green) a distance d from the disc axis. The wheel sits at an angle γ to the slider direction. The slider is fixed to the disc via a spring coefficient k_2 and damping coefficient c_2 , and its equilibrium position lies a distance $\sqrt{d^2 + r_0^2}$ from the disc axis. The wheel's mass is negligible, the slider's mass is m , and the moment of inertia of the top disc is $\Theta = \beta^2 m$. The bottom disc rotates with a constant angular speed ω_0 , with a viscous friction coefficient c_1 between it and the upper disc. All of the parameters so far described are constants.

The most crucial feature of the model is the friction force between the wheel and the steadily rotating bottom disc. The friction force acts perpendicular to the plane of the wheel and has magnitude μ . Inhomogeneities in the force distribution on the contact patch between the bottom disc and the wheel create a torque on the wheel of magnitude μM . The function M models the deformation of a tyre around the wheel, for which different models are available [21, 24, 30]. Most of these tyre models are smooth but include steep gradients that we replace with discontinuities. In this paper we choose the stretched-string tyre model described in Appendix B.

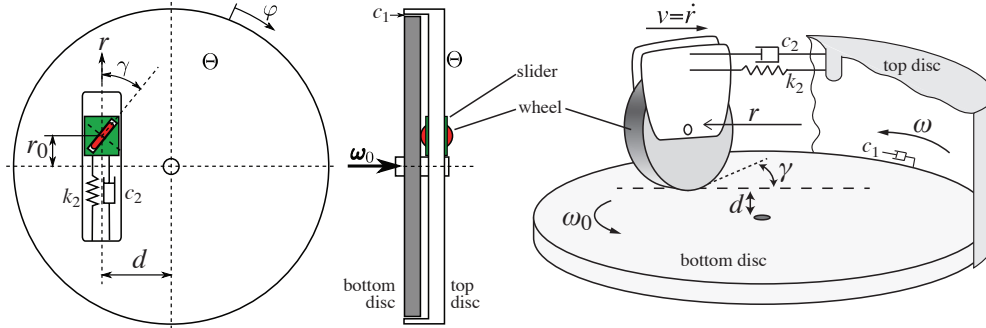


FIG. 1: Mechanical model of the system show from the top (left) and from the side (middle), with a conceptual sketch (right). The bottom disc is rotating with a constant angular speed ω_0 . The top disc rotates around the same centre pin, but it is connected to the bottom disc through a viscous friction coefficient c_1 . A slider is fitted in the top disc, forming a single degree of freedom oscillator. The slider contains a wheel mounted at an angle γ to the slider direction. The wheel is in contact with the bottom disc and Coulomb friction acts between them.

This system can be described using two generalized coordinates, namely the rotation angle of the top disc, φ , and the displacement of the slider, r . Differential equations for the slider displacement r , slider speed $v = \dot{r}$, and the top disc's angular speed $\omega = \dot{\varphi}$, can be derived from the Euler-Lagrange equations (or by directly calculating linear and angular accelerations of the slider and the top disc respectively). These are found to be independent of the angle variable φ , giving the

three dimensional dynamical system

$$\dot{r} = m(\beta^2 + r^2)v, \quad (1)$$

$$\dot{v} = (\beta^2 + d^2 + r^2)p_1(r, v, \omega) - d(c_1 + 2mrv)\omega + F(h, g)p_2(r) + dM(h, g) \quad (2)$$

$$\dot{\omega} = dp_1(r, v, \omega) - (c_1 + 2mrv)\omega + F(h, g)r \cos \gamma + M(h, g), \quad (3)$$

in terms of functions F, M, p_1, p_2, h, g defined below, and where the dot denotes the time derivative. In the equations of motion (1)-(3), time has been rescaled so that the strictly positive quantity $m(\beta^2 + r^2)$ does not appear in the denominator of the righthand side. The functions p_1 and p_2 are given by

$$p_1(r, v, \omega) = k_2(r_0 - r) - c_2v + mr\omega^2, \quad p_2(r) = dr \cos \gamma + (\beta^2 + r^2) \sin \gamma.$$

The functions g and h are the components of the wheel's relative velocity with respect to the bottom disc, in the rolling and the lateral directions, respectively. They are given by

$$h(r, v, \omega) = -(v - d(\omega - \omega_0)) \sin(\gamma) - r(\omega - \omega_0) \cos(\gamma), \quad (4)$$

$$g(r, v, \omega) = -(v - d(\omega - \omega_0)) \cos(\gamma) + r(\omega - \omega_0) \sin(\gamma). \quad (5)$$

When $h = 0$ and $v = 0$, the wheel rolls around the disc in a circle without slipping, such that $r = d \tan \gamma$. When $h = 0$ but $v \neq 0$, the wheel instantaneously rolls on a spiral about the centre of the disc.

The friction force F and moment M represent the tyre model (derived in Appendix B), and are given by

$$F(h, g) = \text{sign}(h)\mu \left(\frac{4}{3} - \frac{\cot \psi}{18\kappa} \right), \quad (6)$$

$$M(h, g) = \text{sign}(g)\text{sign}(h)\frac{\mu}{6} \cot \psi, \quad (7)$$

where $\psi = \text{arccot } 6\kappa + \left|1 - \frac{2}{\pi} \text{arccot } 6\kappa\right| \arctan |h/g|$. An important feature of the model is that $\lim_{h \rightarrow 0^\pm} M = \pm \text{sign}(g)\mu\kappa$, which imparts a nonzero torque on the wheel as it enters the sticking phase $h = 0$.

The system is piecewise-smooth because the friction force F and moment M are discontinuous at $h = 0$. This defines a set of points

$$\Sigma = \{(r, v, \omega) \in \mathbb{R}^3 : h(r, v, \omega) = 0\}$$

called the *switching surface*. When $h \neq 0$, F and M are smooth functions of h and g , so equations (1)-(3) remain smooth and have unique solutions $(r(t), v(t), \omega(t))$. Note that the moment M stays smooth when g changes sign since this occurs when $\psi = \pi/2$ and hence $\cot \psi = 0$.

To solve the equations of motion when they reach the switching surface Σ , we first assume that F and M never exceed the absolute values they have as they approach Σ (i.e. static and kinetic friction are equal), hence $|F| \leq \mu$ and $|M| \leq \mu\kappa$. Only two kinds of solutions are possible given that a trajectory $(r(t), v(t), \omega(t))$ must be a continuous solution of (1)-(2): either a solution will stick to the surface Σ , or it will cross through Σ transversally which reverses the direction of slipping.

The values of F and M during sticking are not fixed by (6)-(7) because the value of $\text{sign}(h)$ is not well-defined at $h = 0$. To establish whether sticking occurs, we ask whether there exists $F \in [-\mu, +\mu]$ such that the vector field (1)-(3) is tangential to Σ . If such an F exists, then sticking occurs and solution follow (1)-(3) along Σ with the given value of F and with $M = \kappa F$. In mechanical terms, evolution along Σ corresponds to stick of the contact surfaces, during which the mechanical constraint $h = 0$ holds. Note that the friction force and moment are tied together during stick by the constant κ . If there exists no value of λ in the interval $[-\mu, +\mu]$ for which (1)-(3) is tangential to Σ , then sticking to Σ is impossible dynamically and trajectories cross from slipping in one direction to the other.

The region of Σ where sticking occurs is reachable from both ‘right slip’ $h > 0$ and ‘left slip’ $h < 0$. It is called the *sliding surface*, because trajectories do not just stick to Σ but evolve or *slide* over its surface as F varies between $[-\mu, +\mu]$ (to avoid confusion note: we employ this mathematical usage of the word ‘slide’ during the stick phase on $h = 0$, and use ‘slip’ to describe non-stick contact in the mechanical sense for $h \neq 0$). The sticking surface a subset of Σ on which the vector field $(\dot{x}, \dot{v}, \dot{\omega})$ points towards $h = 0$ from both $h > 0$ and $h < 0$., hence it is an attractor of the local dynamics. Conversely, it is mathematically possible for an unstable form of sticking to occur on an *escaping surface*, where the vector field $(\dot{x}, \dot{v}, \dot{\omega})$ points away from $h = 0$ from both $h > 0$ and $h < 0$. Thus an escaping region is a repeller of local dynamics, on which sticking occurs but can end spontaneously (or under arbitrarily small perturbations in practice) upon which solutions depart Σ abruptly. This definition seems to imply that solutions will never reach an escaping surface, making it physically uninteresting. That this it not the case was shown in [7], and we illustrate it shortly using the model above. The three basic behaviours — sliding, escaping, and crossing — are illustrated in Figure 2.

Sticking ceases at points where the attractivity of Σ breaks down, namely where $(\dot{r}, \dot{v}, \dot{\omega})$ does not point either towards Σ (for a sliding region) or away from Σ (for an escaping region) from both $h > 0$ and $h < 0$. Thus the conditions

$$\lim_{h \rightarrow 0^\pm} (\dot{r}, \dot{v}, \dot{\omega}) \cdot \nabla h(r, v, \omega) = 0$$

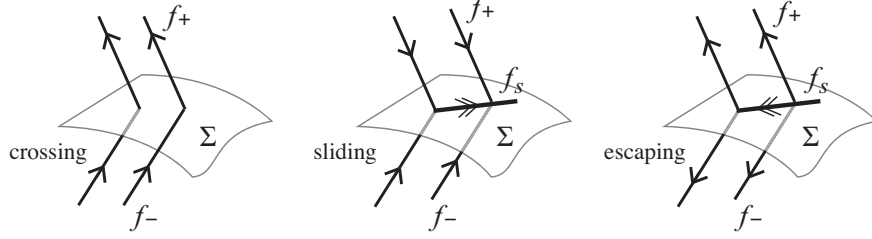


FIG. 2: Typical dynamics as the switching surface: crossing, sliding, and escaping. The limit of (1)-(2) as (r, v, ω) approaches Σ are labelled as $f_{\pm} = \lim_{h \rightarrow 0^{\pm}} (\dot{r}, \dot{v}, \dot{\omega})$. The vector field f_s that governs sticking will be defined in section IV.

define curves bounding regions of sliding or escaping. If these two curves intersect they typically bring sliding and escaping regions together at the intersection point, defined by

$$\lim_{h \rightarrow 0^+} (\dot{r}, \dot{v}, \dot{\omega}) \cdot \nabla h(r, v, \omega) = \lim_{h \rightarrow 0^-} (\dot{r}, \dot{v}, \dot{\omega}) \cdot \nabla h(r, v, \omega) = 0. \quad (8)$$

Despite its low dimension, this point, known as the *two-fold singularity*, will turn out to be highly important to the dynamics. One role it can have is to funnel trajectories from sliding to escaping motion [7], making escaping dynamics an important and observable feature of the system's dynamics. This is the situation found in the device above. Once inside the escaping region, it is impossible to determine from the equations of motion exactly how and where a trajectory will cease sticking. Thus the singularity introduces an interval of non-deterministic motion in an otherwise deterministic system, in which we cannot determine how long sticking will last, or what the slipping motion will look like immediately after, but once slipping motion is restarted then determinism is restored.

These features of crossing and sticking will be formalised in more detail in section IV.

III. SINGULARITY OF THE FRICTION FORCE

The singularity that appears is simple to describe in mechanical terms if we assume that the friction force and moment are related linearly during stick. If the mechanical system can be placed into a configuration where friction force and moment balance each other with respect to the constraints, then due to their linear relation any friction force would balance the moment that is proportional to the force. In the model (1)-(3), this balance occurs via the constraint of the pin holding together the two independently rotating discs. The formal equation (8) exactly describes this situation. It requires stick at a point with two different values of λ , which due to linearity implies that (8) must also hold for any λ , hence M and F are in balance.

The conditions $h = 0$ and (8) for the two-fold singularity give equations that are solveable, but highly nonlinear, in the variables (r, v, ω) . Rather than solving for these in terms of the system parameters, let us say that the singularity lies at coordinates $(r, v, \omega) = (r^*, v^*, \omega^*)$ when two of the parameters of the device, say κ and k_2 , take certain values dependent on (r^*, v^*, ω^*) . We thus solve the equations (8) along with $h(r^*, v^*, \omega^*) = 0$, to find

$$v^* = (\omega^* - \omega_0) (d - r^* \cot \gamma), \quad (9)$$

$$\kappa = -\frac{2r^{*2} + \beta^2 (1 - \cos(2\gamma))}{2r^* \cos \gamma}, \quad (10)$$

$$k_2 = \frac{1}{(r^* - r_0) p_2(r^*, v^*, \omega^*)} \left(\sin(\gamma) (\beta^2 + r^{*2}) (mr^* \omega^{*2} - c_2 v^*) - \cos(\gamma) (c_1 r^* \omega^* + c_2 d r^* v^* + m (r^{*2} (v^* (\omega^* + \omega_0) - d \omega^{*2}) + \beta^2 v^* (\omega_0 - \omega^*))) \right). \quad (11)$$

By solving these numerically one finds at most four singularities on Σ . Only one of these creates non-determinism, as described in the next section.

IV. TEIXEIRA SINGULARITY

There are different types of two-fold singularities [7, 11, 18]. The type responsible for introducing non-determinism to the device above is known as a *Teixeira singularity*, formed where the flow curves inwards towards the switching surface Σ from both sides (see later in Figure 3(left)); in the two other types of two-folds, the flow curves away from the surface on one or both sides. Here we derive the conditions that guarantee a non-degenerate singularity, and moreover give stick motion through the singularity, leading to loss of determinism.

The value of the function $\text{sign}(h)$ in (6)-(7) is ambiguous at $h = 0$. To resolve this we replace the contact force $\mu \text{sign}(h)$ with a variable λ satisfying

$$\lambda(r, v, \omega) \in \mu \times \begin{cases} \text{sign}(h(r, v, \omega)) & \text{if } h(r, v, \omega) \neq 0, \\ [-1, +1] & \text{if } h(r, v, \omega) = 0, \end{cases} \quad (12)$$

and seek conditions to define the value of λ during sticking on $h = 0$. Firstly, note that on $h = 0$ the friction force and moment are tied together as $F = \lambda$ and $M = \kappa \lambda$.

For conciseness let $x = (r, v, \omega)$, and denote the right-hand side of (1)-(3) by $f(x, \lambda)$, giving

$$\dot{x} = f(x, \lambda). \quad (13)$$

The vector field (13) depends linearly on the friction force λ , and we can write

$$\dot{x} = f(x, 0) + \lambda f_\lambda(x, 0),$$

where $f_\lambda(x, 0)$ denotes the partial derivative $\frac{\partial}{\partial \lambda} f(x, \lambda)$, evaluated at $\lambda = 0$. Paraphrasing the statements at the end of section II, we can then find the conditions defining sliding or escaping regions, and find the equations of sticking motion within them.

For sticking motion to occur, the vector field $f(x, \lambda)$ must be able to lie tangent to Σ for admissible values of λ , namely $\lambda \in [-\mu, +\mu]$. This means the h component of f must vanish, or equivalently that the Lie derivative of h with respect to f , must vanish,

$$h_x(x) \cdot (f(x, 0) + \lambda f_\lambda(x, 0)) = 0, \quad (14)$$

with solution

$$\lambda = -\frac{h_x(x) \cdot f(x, 0)}{h_x(x) \cdot f_\lambda(x, 0)}. \quad (15)$$

Using this value for λ the equations of motion for sticking become

$$\dot{x} = f(x, 0) - \frac{h_x(x) \cdot f(x, 0)}{h_x(x) \cdot f_\lambda(x, 0)} f_\lambda(x, 0). \quad (16)$$

This is known as the *sliding vector field* in piecewise-smooth dynamical systems theory [8, 11]. In mechanical terms, evolution along Σ corresponds to stick of the contact surfaces, during which the mechanical constraint $h = 0$ holds. (We re-iterate that the word ‘slide’ is used to describe evolution on $h = 0$ during the stick phase, and ‘slip’ is used to describe non-stick contact in the mechanical sense for $h \neq 0$). Then λ is the static friction force, as calculated from the equations of motion. If there are no values of λ in the interval $[-\mu, +\mu]$ such that (14) is satisfied, then sticking to Σ is impossible dynamically and solutions must cross Σ transversally from left slip, $h < 0$, to right slip, $h > 0$.

A sliding region, where sticking occurs so (15) lies inside $[-\mu, +\mu]$ and Σ is attractive, now satisfies

$$-h_x(x) \cdot f_\lambda(x, 0) > h_x(x) \cdot f(x, 0)/\mu > h_x(x) \cdot f_\lambda(x, 0). \quad (17)$$

An escaping region, where sticking occurs and Σ is repulsive, satisfies

$$-h_x(x) \cdot f_\lambda(x, 0) < h_x(x) \cdot f(x, 0)/\mu < h_x(x) \cdot f_\lambda(x, 0). \quad (18)$$

The boundaries of sliding or escaping regions hence lie where

$$h_x(x) \cdot f(x, 0) = \pm \mu h_x(x) \cdot f_\lambda(x, 0).$$

If both of these equations hold, then two boundaries intersect at a point, which we label x^* , where

$$h_{x^*}(x^*) \cdot f(x^*, 0) = h_{x^*}(x^*) \cdot f_\lambda(x^*, 0) = 0. \quad (19)$$

This is the two-fold singularity. Generically the intersection of the two boundaries is transversal, meaning $f(x^*, 0)$ and $f_\lambda(x^*, 0)$ are linearly independent, as well as both tangent to Σ . At x^* , both the numerator and the denominator of the fraction in (16) vanish, and so the sliding vector field is ill-defined. The problem is easily dealt with by considering the scaled vector field

$$(h_x(x) \cdot f_\lambda(x, 0)) \dot{x} = h_x(x) \cdot f_\lambda(x, 0) f(x, 0) - h_x(x) \cdot f(x, 0) f_\lambda(x, 0). \quad (20)$$

The right-hand side is a vector field which is a positive scaling of (16) in the sliding region, a scaling of (16) with directions reversed in the escaping region, and with a zero at the singularity (see e.g. [7]). We are interested in the dynamics local to the singularity, so we linearize equation (20) at x^* , which yields

$$(\partial_x (h_x \cdot f_\lambda) x) \dot{x} = f \partial_x (h_x \cdot f_\lambda) x - f_\lambda \partial_x (h_x \cdot f) x + O(|x|^2) \quad (21)$$

(omitting the arguments of $h = h(x)$, $f = f(x, 0)$ and $f_\lambda = f_\lambda(x, 0)$ for brevity).

The vector field on the right side of (21) spans two dimensions (the tangent plane to Σ), since $f(x^*, 0)$ and $f_\lambda(x^*, 0)$ are linearly independent. Therefore it is sensible to parameterize the perturbation as $x = \alpha f(x, 0) + \beta f_\lambda(x, 0) + y$, where y can be chosen from the kernel of (21), and α, β , are parameters. In particular there is a projection P such that $y = Px$. Let us define

$$\begin{aligned} \mathcal{K}^{++} &= \partial_x (h_x \cdot f(x, +\mu)) \cdot f(x, +\mu), & \mathcal{K}^{+-} &= \partial_x (h_x \cdot f(x, +\mu)) \cdot f(x, -\mu), \\ \mathcal{K}^{-+} &= \partial_x (h_x \cdot f(x, -\mu)) \cdot f(x, +\mu), & \mathcal{K}^{--} &= \partial_x (h_x \cdot f(x, -\mu)) \cdot f(x, -\mu), \end{aligned} \quad (22)$$

The boundaries of the sticking regions are found by substituting $\lambda = \pm\mu$ into (14). Linearizing this constraint we find

$$\partial_x (h_x \cdot (f(x, 0) \pm \mu f_\lambda(x, 0))) (\alpha^\pm f(x, 0) + \beta^\pm f_\lambda(x, 0)) + O(|x|^2) = 0. \quad (23)$$

To leading order this is satisfied if

$$\begin{aligned} \alpha^\pm &= \partial_x (h_x \cdot (f(x, 0) \pm \mu f_\lambda(x, 0))) f_\lambda(x, 0) = \frac{1}{2\mu} (\mathcal{K}^{\pm+} - \mathcal{K}^{\pm-}), \\ \beta^\pm &= -\partial_x (h_x \cdot (f(x, 0) \pm \mu f_\lambda(x, 0))) f(x, 0) = -\frac{1}{2} (\mathcal{K}^{\pm-} + \mathcal{K}^{\pm+}). \end{aligned}$$

The pair of vectors $v^\pm = \alpha^\pm f(x, 0) + \beta^\pm f_\lambda(x, 0)$ can now be defined as natural coordinates for the linearised sticking motion, that is, $x = \xi v^+ + \eta v^- + y$ where ξ and η are coordinates measured along the v^+ and v^- directions. In these coordinates the linearization of the time-scaled sliding vector field (21) becomes

$$(\xi + \eta) (\dot{\xi} v^+ + \dot{\eta} v^- + \dot{y}) = (f(x, 0)(\xi + \eta) + \mu f_\lambda(x, 0)(\xi - \eta)). \quad (24)$$

We also evaluate the time derivatives to get

$$\begin{aligned} \dot{\xi}v^+ + \dot{\eta}v^- = \frac{1}{2\mu} \Big\{ & f(x, 0) \left((\mathcal{K}^{++} - \mathcal{K}^{+-}) \dot{\xi} + (\mathcal{K}^{-+} - \mathcal{K}^{--}) \dot{\eta} \right) \\ & - \mu f_\lambda(x, 0) \left((\mathcal{K}^{+-} + \mathcal{K}^{++}) \dot{\xi} + (\mathcal{K}^{--} + \mathcal{K}^{-+}) \dot{\eta} \right) \Big\}. \end{aligned} \quad (25)$$

Substituting (25) into (24) and solving for the derivatives $\dot{\xi}, \dot{\eta}, \dot{y}$ yields

$$\begin{aligned} \dot{\xi} &= -\frac{2\mu}{a(\xi, \eta)} (\mathcal{K}^{-+}\xi + \mathcal{K}^{--}\eta), \\ \dot{\eta} &= \frac{2\mu}{a(\xi, \eta)} (\mathcal{K}^{++}\xi + \mathcal{K}^{+-}\eta), \\ \dot{y} &= 0, \end{aligned} \quad (26)$$

where $a(\xi, \eta) = (\mathcal{K}^{-+}\mathcal{K}^{+-} - \mathcal{K}^{++}\mathcal{K}^{--})(\eta + \xi)$.

Equation (26) describes the dynamics on the switching surface. We must also establish how a trajectory might arrive at the switching surface. Let us assume that the two-fold singularity of interest is a Teixeira singularity [7, 17], meaning the flows curve towards Σ at the boundaries of sticking (figure 3). This implies

$$\mathcal{K}^{++} < 0 < \mathcal{K}^{--}. \quad (27)$$

The sliding region satisfies (17), whose linearization is $\partial_x(h_x \cdot f(x, \mu))x < 0 < \partial_x(h_x \cdot f(x, -\mu))x$.

This means sliding occurs for values of ξ and η that satisfy

$$\frac{\eta}{2\mu} (\mathcal{K}^{-+}\mathcal{K}^{+-} - \mathcal{K}^{++}\mathcal{K}^{--}) < 0 < \frac{-\xi}{2\mu} (\mathcal{K}^{-+}\mathcal{K}^{+-} - \mathcal{K}^{++}\mathcal{K}^{--}). \quad (28)$$

Similarly escaping occurs for values

$$\frac{-\xi}{2\mu} (\mathcal{K}^{-+}\mathcal{K}^{+-} - \mathcal{K}^{++}\mathcal{K}^{--}) < 0 < \frac{\eta}{2\mu} (\mathcal{K}^{-+}\mathcal{K}^{+-} - \mathcal{K}^{++}\mathcal{K}^{--}). \quad (29)$$

Two crucial constants characterize the local dynamics,

$$\mathcal{J}_1 = \frac{\mathcal{K}^{-+}}{\sqrt{-\mathcal{K}^{++}\mathcal{K}^{--}}}, \quad \text{and} \quad \mathcal{J}_2 = -\frac{\mathcal{K}^{+-}}{\sqrt{-\mathcal{K}^{++}\mathcal{K}^{--}}}.$$

If we choose scaled coordinates $(\bar{\xi}, \bar{\eta}) = (\xi, \eta)\sqrt{\frac{\mathcal{K}^{++}}{\mathcal{K}^{--}}}$, and rescale time by $\bar{t} = t\sqrt{-\mathcal{K}^{++}\mathcal{K}^{--}}$, the local system simplifies to

$$\begin{pmatrix} \dot{\bar{\xi}} \\ \dot{\bar{\eta}} \end{pmatrix} = \frac{1}{(\mathcal{J}_1\mathcal{J}_2 - 1)(\bar{\eta} + \bar{\xi})} \begin{pmatrix} \mathcal{J}_1 & 1 \\ 1 & \mathcal{J}_2 \end{pmatrix} \begin{pmatrix} \bar{\xi} \\ \bar{\eta} \end{pmatrix}. \quad (30)$$

Using condition (28) we find that if $\mathcal{J}_1\mathcal{J}_2 - 1 > 0$ then the sliding region is simply $\xi > 0, \eta > 0$, and $\xi < 0, \eta < 0$ otherwise. A simple time-rescaling guarantees the former case, transforming (30) into

$$\begin{pmatrix} \dot{\bar{\xi}} \\ \dot{\bar{\eta}} \end{pmatrix} = \frac{1}{\bar{\eta} + \bar{\xi}} \begin{pmatrix} \mathcal{J}_1 & 1 \\ 1 & \mathcal{J}_2 \end{pmatrix} \begin{pmatrix} \bar{\xi} \\ \bar{\eta} \end{pmatrix}.$$

Note that given condition (27) the eigenvalues of the matrix in (30) are real, and given by

$$\lambda_{1,2} = \frac{1}{2} \left(\mathcal{J}_1 + \mathcal{J}_2 \pm \sqrt{(\mathcal{J}_1 - \mathcal{J}_2)^2 + 4} \right),$$

with associated eigenvectors

$$v_{1,2} = \begin{pmatrix} \lambda_{1,2} - \mathcal{J}_2 \\ 1 \end{pmatrix}.$$

The first eigenvector points into the sliding region, while the second eigenvector points into the crossing region. One of the eigenvalues become zero if $1 = \mathcal{J}_1\mathcal{J}_2$. The eigenvalues cannot be equal, but they can have the same magnitude with different sign if $\mathcal{J}_2 + \mathcal{J}_1 = 0$. Depending on the values of $\mathcal{J}_1, \mathcal{J}_2$ we have three cases [7, 17]:

1. If $\mathcal{J}_1, \mathcal{J}_2 < 0$ and $\mathcal{J}_1\mathcal{J}_2 > 1$ both eigenvalues are negative, so the singularity attracts trajectories from the sliding region, and repels them into the escaping region. The eigenvector in the sliding region is weak stable compared to the eigenvector in the crossing region, which implies that trajectories from the sliding region all approach the weak eigenvector direction, and hence all flow into the singularity.
2. If $\mathcal{J}_1, \mathcal{J}_2 > 0$ and $\mathcal{J}_1\mathcal{J}_2 > 1$ both eigenvalues are positive, the singularity is repelling from the sliding region and attracting from the escaping region.
3. When $\mathcal{J}_1\mathcal{J}_2 > 1$ one eigenvalue is positive, the other negative, the singularity is repelling from the sliding region and attracting from the escaping region.

In terms of our mechanical system case 1 is the most interesting, because all sliding trajectories in the vicinity of the singularity will reach x^* . This is illustrated in Figure 3.

The local dynamics is illustrated by a few typical trajectories in Figure 3. Trajectories repeatedly wind around the singularity through sequences of switchings and stickings, such that even the local dynamics can be somewhat complex, and a fuller description can be found in [7, 17]. For the mechanical system of interest, simulations show that trajectories spend only a short amount

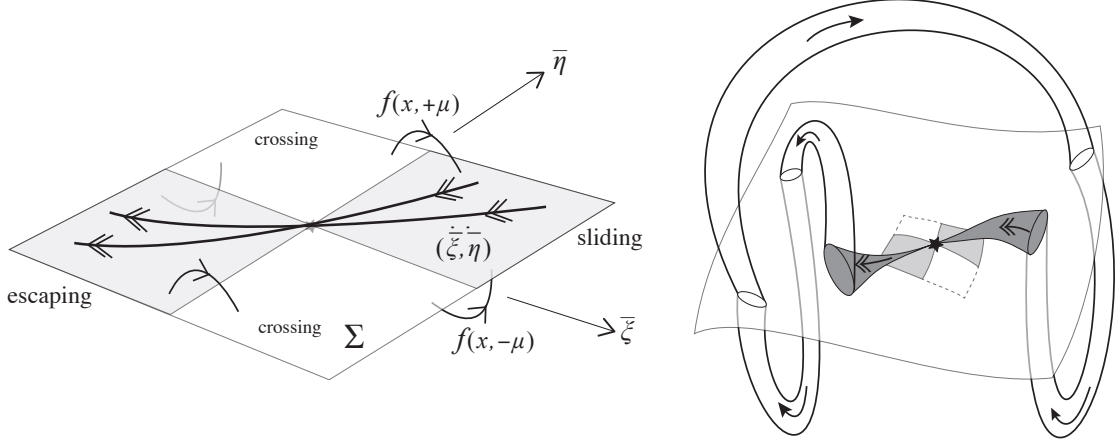


FIG. 3: Non-determinism at a Teixeira singularity. *Left*: Slipping (single-headed arrows) follows $f(x, +\mu)$ or $f(x, -\mu)$ either side of the switching surface. Sticking (double arrows) follows $(\dot{\xi}, \dot{\eta})$ in the sliding and escaping regions (shaded). In the case shown, the sticking flow passes through the singularity non-deterministically. *Right*: Sketch of non-deterministic chaos in the mechanical system. The small shaded “bow-tie” shows the local region of the singularity (shown left). A set of trajectories loop around via a sequence of slipping (white bands) with switches, connecting to the singularity via sticking (dark band) in both forward and backward time.

of time near the singularity. In doing so they can travel through the singularity itself, and what happens at that point is non-deterministic: a continuous set of future trajectories are possible.

The problem of unpredictability could be neglected if it affected only a single point. In this system that is not the case for two reasons. Firstly, whole sets of solutions evolve into the singularity. Secondly, even after solutions have left the singularity, the global dynamics can cause their trajectories to return to the singularity again. This creates a set of closed solutions that return repeatedly to the singularity, even though which trajectory they follow within that set cannot be determined. The motion therefore inhabits a chaotic set generated by non-determinism at the singularity. A simplification of this feedback mechanism is sketched in Figure 3(right). In the next section we simulate this non-deterministic chaos in the mechanical model and give parameters for which it occurs.

V. SIMULATIONS OF THE MECHANICAL MODEL

A number of conditions must be satisfied for the system (13) to lead to non-determinism and chaos. The presence of a Teixeira singularity exhibiting non-determinism is guaranteed from (27) if $\mathcal{J}_1 < 0$, $\mathcal{J}_2 < 0$ and $\mathcal{J}_1\mathcal{J}_2 > 1$ all hold. If we fix the constants $d = 1$, $m = 1$, $c_1 = c_2 = 10^{-3}$,

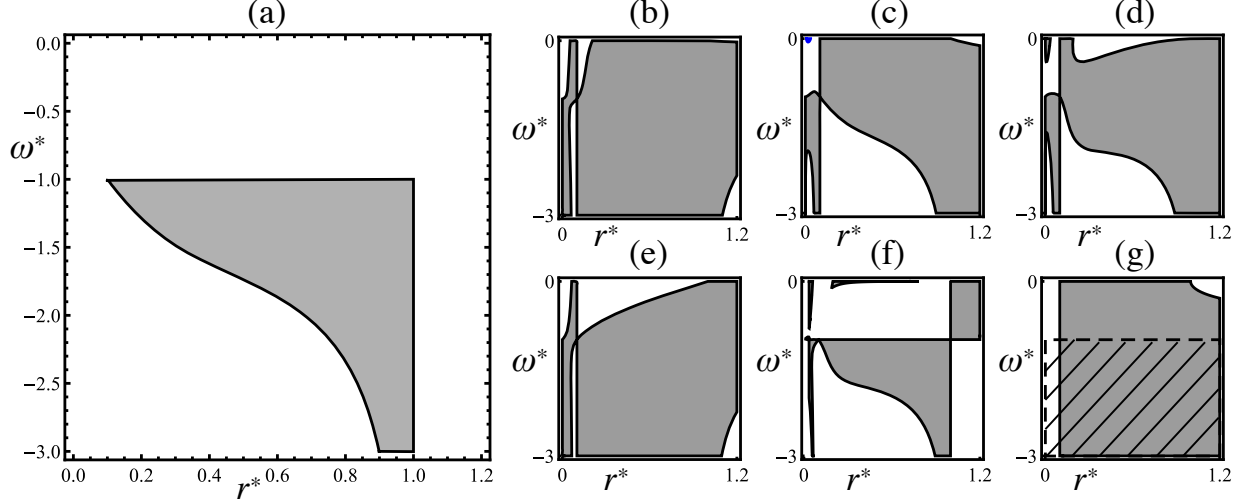


FIG. 4: The shaded region in panel (a) represents parameter values where the system has a Teixeira singularity (case 1 in section IV). This is the overlap of several conditions: (b) $\mathcal{K}^{--} > 0$, (c) $\mathcal{K}^{++} < 0$, (d) $\mathcal{J}_1 < 0$, (e) $\mathcal{J}_2 < 0$, (f) $\mathcal{J}_1\mathcal{J}_2 - 1 > 0$, and in (g) showing both $k_2 > 0$ (shaded) and $\kappa > 0$ (hatched).

$\beta = \frac{1}{20}$, $r_0 = 10^{-1}$, $\omega_0 = -1$, $\mu = 1$ and $\gamma = -\frac{3}{4}\pi$, then there exist regions of r^* and ω^* values satisfying these conditions, as illustrated in Figure 4. In general there are large regions in parameter space where the required conditions are satisfied, and while not all will also yield the recurrent dynamics required for chaos, it is not difficult to find parameters that do.

Within the shaded area in Figure 4(a) we choose $r^* = 0.1859$ and $\omega^* = -1.037$ and use the numerical method described in [26] to compute trajectories of the piecewise-smooth system. The top left panel of Figure 5 shows the switching surface around the singularity on the sliding surface. The sliding surface is indicated by the grey region where the green and red shaded regions overlap. The non-overlapping green and red regions are where trajectories cross the switching surface Σ . The white area indicates the escaping surface. It can be seen that trajectories from the bottom right sliding surface will pass through the singularity, while the trajectories of the top sliding surface connect the escaping surface with the middle crossing region.

The full simulation is shown in the top left and bottom panels of Figure 5(b). The figures shows that sticking trajectories that cross the singularity arrive in the escaping region and get repelled by it. After leaving the escaping region trajectories go into a outward spiraling motion and cross the switching surface until that ceases to exists and arrive at the other sliding surface. Eventually the solution starts to slip again to end up in the sliding surface of the singularity to start the cycle again. Because of the non-determinism at the singularity the cycles are not identical, hence the attractor is not a periodic orbit, but a full surface of solutions. The basin of attraction of

this set of solutions is not the entire phase space. In fact it is even possible that the recurrent non-deterministic phenomena is only transient, because the non-deterministic effect can also push the trajectory out towards a different attractor.

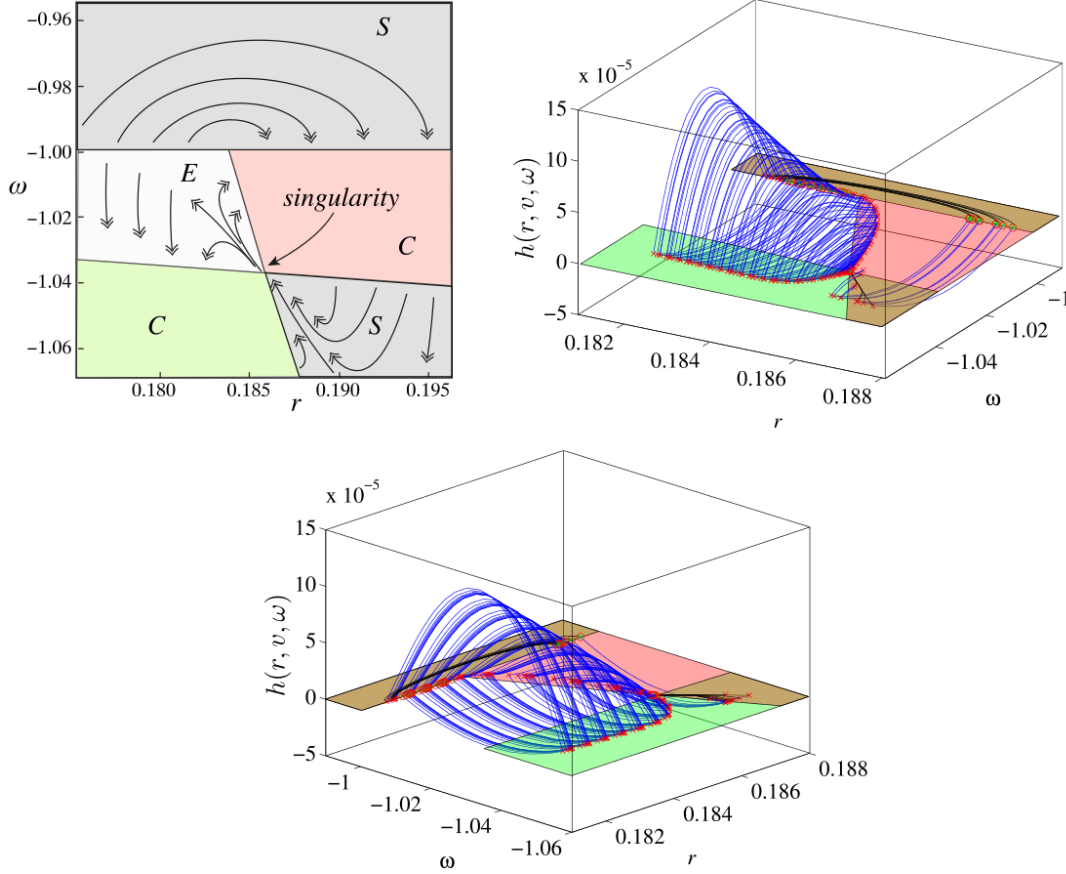


FIG. 5: Non-deterministic chaos in the wheel-and-disc assembly for parameter values given in the text. Top left panel: a sketch of the sticking flow, showing sliding regions (S), escaping region (E), and crossing regions (C). A Teixeira singularity is seen at $(r, \omega) = (0.1859, -1.037)$, with the sticking flow passing through it along a weak eigenvector. The 3D blocks show a simulation of different trajectories with initial conditions near the escaping region (regions on $v = 0$ correspond to those in the top-left panel; colour online). These represent the different trajectories followed after passing through the singularity. The trajectories wind around the escaping region causing the dense shell seen in $r < 0.1859$.

These trajectories are not simulated actually passing through the singularity, as such a simulation is impossible by the very definition of the singularity. When a trajectory enters the singularity (as every trajectory in figure 5 does), the simulation must be stopped and a decision must be made on which of the infinity of possible trajectories to follow. Since all of these pass through the escaping region at least briefly, we simply select a new starting condition near the escaping surface, and by following these we begin to trace out the cone-like form of the non-deterministic chaotic

set, and show at least that all such trajectories find their way eventually back into the singularity via the sliding region.

VI. SPECIAL CASES: SINGULARITY WITHOUT NON-DETERMINISM

A. The case $\gamma = 0$

When $\gamma = 0$ the wheel is mounted so that its axis is perpendicular to the slider. As a result, when $r = 0$ the wheel rolls without slipping around the lower disc in a circle of radius d . If r is nonzero the wheel will typically slip except when the upper and lower discs rotate in unison, which is when $\omega = \omega_0$. Thus the sticking surface is $h = r(\omega_0 - \omega)$, as is found by substituting $\gamma = 0$ in (4).

The equations for a two-fold singularity (8) then have only one valid solution where $r^* = \kappa$, $\omega^* = \omega_0$, and $v^* = \left(d[\frac{k_2}{m}(\kappa + r_0) - \kappa\omega_0^2] - \frac{c_1}{m}\omega_0\right) / (d\frac{c_2}{m} - 2\kappa\omega_0)$. Although this is a two-fold singularity, it is a special case in which $f(x^*, +\mu) = f(x^*, -\mu)$, since substituting $\gamma = 0$ and $r = -\kappa$ into (1)-(3) causes the $\text{sign}(h)$ terms to drop out. Hence the system is continuous, and uniquely defined, precisely at the singularity. This is a special case of the singularity presented in the previous section, where non-determinism vanishes as γ is taken to 0.

B. The case $\gamma = \pi/2$

When $\gamma = \pi/2$ the wheel is mounted with its axis lying along the slider. If the wheel sticks then its speed in the slider v must be equal to the mismatch in the speed of the discs, $d(\omega - \omega_0)$, and substituting $\gamma = \pi/2$ into (4) gives $h = d(\omega - \omega_0) - v$. There are no two-fold singularities because the sticking boundaries form non-intersecting curves. This is a common situation in simple mechanical models, where the expressions for $f(x, \pm\mu)$ differ only by a constant 2μ , so the boundaries between sticking and slipping given by $h = f(x, \pm\mu) = 0$ are displaced by an amount 2μ . The boundaries can only meet when $\mu = 0$, in which case there is no friction force and no discontinuity.

VII. CLOSING REMARKS

Unlike an abstract model in [19] contrived to demonstrate the potential for mechanical models exhibiting non-deterministic chaos, the model presented here is based on fundamental mechanical principles which themselves have far wider applications. The essential characteristics of the model

are a coupling of linear and angular motions, and the sudden change of force that occurs in dry friction. It is therefore reasonable to suggest that the two-fold singularity may be common wherever such features occur in physical applications. Uncertainty in the dynamics from a particular configuration may now be recognized as a local breakdown of determinism (whether it repeats to give chaotic dynamics or not), inherent in the physical geometry.

In this local aspect, the non-deterministic chaotic dynamics here is very different to standard explanations for the phenomenon of wheel shimmy or flutter, a problem familiar to anyone who has wrestled with an unwieldy shopping trolley. Current explanations for this tend to involve smooth deterministic oscillations around the ideal alignment of a wheel. These do share some aspects with the non-deterministic effect in this paper, in that violent oscillations of the wheel are a result of coupling of linear and rotational motion due to nonlinearities from the wheel (or tyre) elasticity. Where they differ is that our model involves unpredictability in the transition through a singular configuration, and it is discontinuities in the dry-friction model, more severe than nonlinearity, that create such determinism destroying singularities. (We should note here that our system is not intended to model shimmy, since it involves a wheel at a fixed angle moving around a disc, while shimmy involves a wheel with varying angle moving along a line; our model is designed only to investigate the phenomenon of non-deterministic chaos).

In the simulations in section V, it is not actually possible to follow the trajectories through the singularity, because by definition their evolution becomes non-deterministic there. Many possibilities can be argued for how to follow the simulation through the singularity, perhaps by smoothing out the sign functions in (6)-(7), or by choosing one of the possible trajectories probabilistically assuming some stochastic distribution. The smoothing approach produces a stiff model that is very sensitive to the functional form of the smoothing, to choices of parameters and to initial conditions, and sensitive to machine precision used in the simulation. Such simulations were made on a simplified version of this model in [16]. The stochastic approach has not been studied to date, as there is no obvious way to choose an appropriate distribution based on likely noise input into the system, however such an investigation would be of great interest. Preliminary investigations such as [16] suggest that, as expected, however noisy or unpredictable the output of such smoothed or stochastic systems, they do indeed constitute a sample of the trajectories observed in the discontinuous model, i.e. in figure 5.

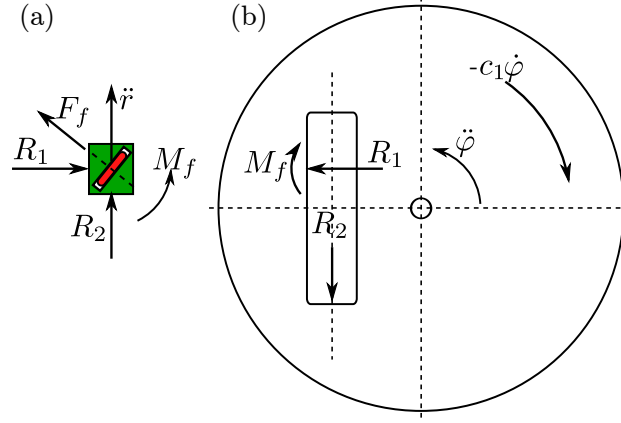


FIG. 6: Free-body diagrams of the mechanical system.

Appendix A. Equations of motion

Consider the system as illustrated by the schematic in Fig. 1. In order to derive the equations of motions we consider the free-body diagrams of each part in Fig. 6. The generalized coordinates are the rotation angle φ of the top disc and the relative displacement r of the slider within the disc. Using these coordinates we calculate the acceleration of the slider in two directions and apply Newton's law to find the equations of motion. The acceleration of the slider perpendicular to the slit appears in

$$m(-r\ddot{\varphi} + d\dot{\varphi}^2 - 2\dot{r}\dot{\varphi}) = R_1 + F(h, g) \cos \gamma, \quad (31)$$

where R_1 is the reaction force between the slider and the slit and $F(h, g)$ is the friction force between the wheel and the turntable. Parallel to the slit the motion is governed by

$$m(\ddot{r} - d\ddot{\varphi} - r\dot{\varphi}^2) = R_2 - F(h, g) \cos \gamma, \quad (32)$$

where $R_2 = -k_2(r - r_0) - c_2\dot{r}$ is the reaction force in the spring and damper. The angular acceleration of the disc is

$$\Theta\ddot{\varphi} = -c_1\dot{\varphi} + dR_2 + rR_1 + M(h, g), \quad (33)$$

where $M(h, g)$ is the re-aligning moment of the wheel due to friction. The functions h and g are defined by equations (4) and (5) with $\omega = \dot{\varphi}$ and $v = \dot{r}$.

Eliminating the reaction forces and rearranging equations (31,32,33) we arrive at (1,2,3). The friction force $F(h, g)$ and moment $M(h, g)$ are derived in the following appendix.

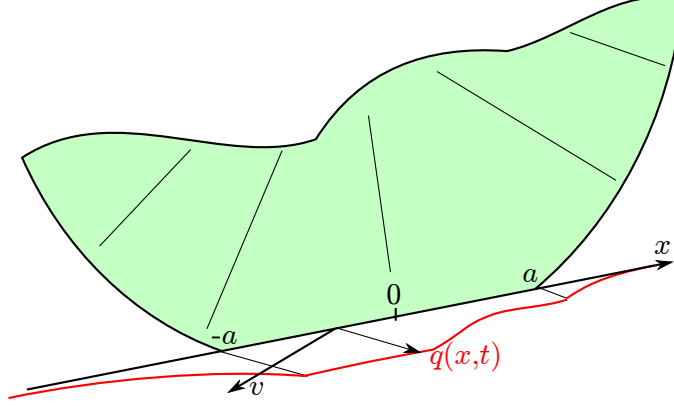


FIG. 7: Contact forces on a rolling wheel. The ground surface is moving with relative velocity v under the wheel, whose lateral deformation is described by $q(x, t)$ within the contact patch spreading from $x = -a$ to $x = a$.

Appendix B. Friction force on the rolling and slipping wheel

The friction forces acting on the wheel are found as follows. We use the stretched string tyre model described in [30] to derive lateral friction forces and the aligning torque. The schematic of the model can be seen in Figure 7.

The deformation of the tyre is characterized by the lateral movement of its central line with respect to its resting position by $q(x)$. We assume that the lateral contact pressure distribution acting on the tyre is proportional to the displacement that is $p(x) = kq(x)$, hence the lateral force is

$$F = k \int_{-a}^a q(x) dx,$$

where k is the lateral stiffness of the tyre. There is also a torque that is trying to rotate the wheel back into a position parallel to the velocity v and that can be calculated for the origin as

$$M = -k \int_{-a}^a xq(x) dx.$$

To determine the shape of $q(x)$ we recall that in case of rolling the contact point has the same velocity as the ground surface. Also, we assume that the direction of the wheel and ground velocity v has a φ angle between them. We are interested in the static deformation, therefore the following constraint holds

$$0 = v \sin \varphi + v \frac{\partial}{\partial x} q(x) \cos \varphi. \quad (34)$$

The boundary condition is specified at the leading edge $\sigma \frac{\partial}{\partial x} q(x) = -q(a)$, where σ is a relaxation constant that specifies how the tyre deformation relaxes when it is not in contact with the ground.

Solving (34) we find that $q(x) = q_0 - x \tan \varphi$. From the boundary condition we calculate that $q_0 = (a + \sigma) \tan \varphi$, therefore the steady state deformation when the wheel is rolling becomes

$$q(x) = (a + \sigma - x) \tan \varphi.$$

To account for a possible slip the distributed friction force $p(x)$ must be limited. We assume static and dynamic friction, where the maximal static lateral pressure is δ and the dynamic pressure is $\rho\delta$, $0 < \rho \leq 1$. This implies that the deformation of the tyre is limited by the maximal friction pressure δ . Solving $k|q(x_s)| = \delta$ for x_s , we find that $x_s = a + \sigma - \frac{\cot \varphi}{k}$. Depending on the value of x_s three cases are possible:

1. $x_s \leq -a$, that is, there is no slip. In this case $F = -2ak(a + \delta) \tan \varphi$, $M = \frac{2}{3}a^3k \tan \varphi$
2. $-a < x_s < a$ implies partial slip, therefore $F = \delta(2a + \sigma) + \frac{\delta^2}{2k}(1 - 2\rho) \cot \varphi - \frac{1}{2}k\sigma^2 \tan \varphi$,

$$M = \frac{k^3\sigma^2(3a + \sigma) \tan \varphi + \delta^2 \cot(\varphi)(2\delta \cot \varphi - 3k(a + \sigma))}{6k^2} - \frac{1}{2}\delta\rho \left(\left(a - \frac{\delta \cot \varphi}{k} + \sigma \right)^2 - a^2 \right)$$
3. $a \leq x_s$ means complete slip, so that $F = 2a\delta$, $M_z = 0$.

As a simplification we choose $\sigma = 0$, $\rho = 2/3$, $\delta = (3\kappa)^{-1}$ and $a = 3\kappa$, where κ is a length scale. This choice of parameters implies that the tyre is infinitely flexible for bending, its stiffness is the same as the maximum static friction pressure and a and δ are chosen such that $F = 1$ and $M = \kappa$ when $x_s = -a$. Using these values we get

$$F = \begin{cases} 18k\kappa^2 \tan \varphi \\ \frac{4}{3} - \frac{\cot \varphi}{54k\kappa^2} \end{cases}, \quad M = \begin{cases} 18k\kappa^3 \tan \varphi & \text{if } 0 \leq \varphi < \cot^{-1}(18k\kappa^2) \\ \frac{\cot \varphi}{18k\kappa} & \text{if } \cot^{-1}(18k\kappa^2) \leq \varphi \leq \frac{\pi}{2} \end{cases}.$$

Choosing some parameters the friction force and torque is plotted in Fig. 8(a). Note that this characteristic is rather similar to Pacejka's empirical magic formula. It can be seen that the initial part of the F and M curves have a steep gradient. In order to impart the non-smooth phenomena we replace this initial section by a discontinuity as shown in Fig. 8(b). The scaling is $\varphi \rightarrow \cot^{-1}(18k\kappa^2) + \varphi \left(1 - \frac{2 \cot^{-1}(18k\kappa^2)}{\pi} \right)$.

-
- [1] F. Al-Bender, V. Lampaert, and J. Swevers. A novel generic model at asperity level for dry friction force dynamics. *Tribology Letters*, 16(1):81–93, 2004.
- [2] M. T. Bengisu and A. Akay. Stick-slip oscillations: Dynamics of friction and surface roughness. *J. Acoust. Soc. Am.*, 105(1):194–205, 1999.

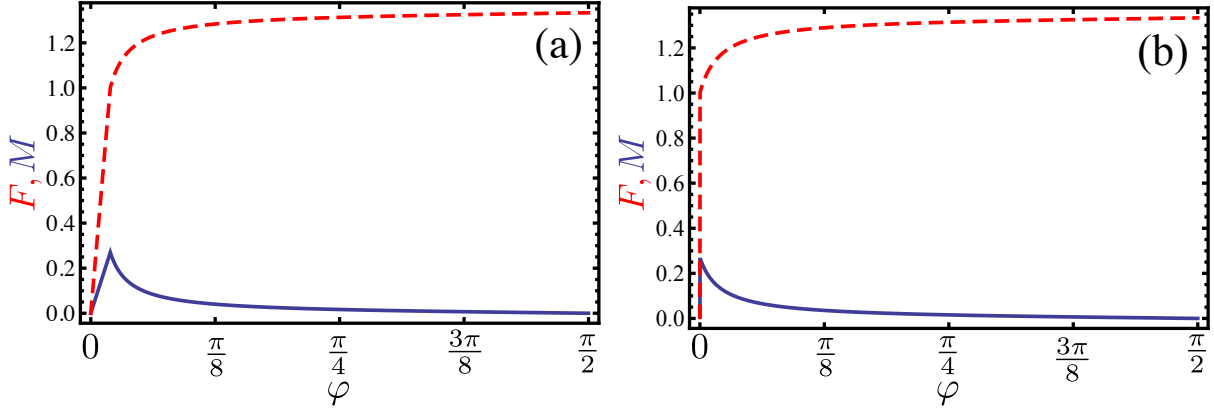


FIG. 8: Plot of the friction force (dashed red lines) and moment (solid blue lines) as a function of slip angle φ . Parameters for the left panel are $k = 1$, $\delta = 1$, $\sigma = 1$ and $a = 1$, for right panel are $k = 10^3$, $\delta = 10^{-3}$, $\sigma = 10^{-3}$ and $a = 1$.

- [3] B. Bhushan. Contact mechanics of rough surfaces in tribology: multiple asperity contact. *Tribology Letters*, 4:1–35, 1998.
- [4] B. Brogliato. *Impact in mechanical systems - analysis and modelling*, volume 551 of *Lecture Notes in Physics*. Springer-Verlag (New York), 2000.
- [5] A. R. Champneys, H. Dankowicz, and A. Nordmark. Friction-induced reverse chatter in rigid-body mechanisms with impacts. *IMA Journal of Applied Mathematics*, 76(1):85–119, 2011.
- [6] A. Colombo, M. di Bernardo, E. Fossas, and M. R. Jeffrey. Teixeira singularities in 3D switched feedback control systems. *Systems & Control Letters*, 59(10):615–622, 2010.
- [7] A. Colombo and M. R. Jeffrey. Non-deterministic chaos, and the two-fold singularity in piecewise smooth flows. *SIAM J. App. Dyn. Sys.*, 10:423–451, 2011.
- [8] M. di Bernardo, C. J. Budd, A. R. Champneys, and P. Kowalczyk. *Piecewise-Smooth Dynamical Systems: Theory and Applications*. Springer, 2008.
- [9] M. di Bernardo, A. Colombo, and E. Fossas. Two-fold singularity in nonsmooth electrical systems. *ISCAS*, pages 2713–2716, 2011.
- [10] D. Dowson. *History of Tribology*. Professional Engineer Publishing, London, 1998.
- [11] A. F. Filippov. *Differential Equations with Discontinuous Righthand Sides*. Kluwer Academic Publ. Dordrecht, 1988.
- [12] D. P. Hess and A. Soom. Normal vibrations and friction under harmonic loads i-ii. *J. Tribol.*, 113(1):80–86, 87–92, 1991.
- [13] J. Ing, E. Pavlovskaya, M. Wiercigroch, and S. Banerjee. Bifurcation analysis of an impact oscillator with a one-sided elastic constraints near grazing. *Physica D*, 239:312–321, 2010.
- [14] M. R. Jeffrey. Non-determinism in the limit of nonsmooth dynamics. *Physical Review Letters*, 106(25):254103, 2011.

- [15] M. R. Jeffrey. Errors and asymptotics in the dynamics of switching. *submitted*, 2013.
- [16] M. R. Jeffrey. Singularities that induce a breakdown of determinism in mechanics. *Proc. 5th International Conference on Structural Dynamics SEMC, 2-4 Sept. 2013*, 2013.
- [17] M. R. Jeffrey and A. Colombo. The two-fold singularity of discontinuous vector fields. *SIAM Journal on Applied Dynamical Systems*, 8(2):624–640, 2009.
- [18] M. R. Jeffrey and S. J. Hogan. The geometry of generic sliding bifurcations. *SIAM Review*, 53(3):505–525, 2011.
- [19] Mike R. Jeffrey. Nondeterminism in the limit of nonsmooth dynamics. *Phys. Rev. Lett.*, 106:254103, 2011.
- [20] J. Krim. Friction at macroscopic and microscopic length scales. *Am. J. Phys.*, 70:890–897, 2002.
- [21] E. Kuiper and J. J. M. Van Oosten. The PAC2002 advanced handling tire model. *Veh. Syst. Dyn.*, 45(S):153–167, 2007.
- [22] A. Le Bot and E. Bou Chakra. Measurement of friction noise versus contact area of rough surfaces weakly loaded. *Tribology Letters*, 37:273–281, 2010.
- [23] H Olsson, K J Astrom, C C de Wit, M Gafvert, and P Lischinsky. Friction models and friction compensation. *Eur. J. Control*, 4(3):176–195, 1998.
- [24] H. B. Pacejka. *Tire and Vehicle Dynamics*. SAE International, 2006.
- [25] B. N. J. Persson. *Sliding Friction: Physical Principles and Applications*. Springer, 1998.
- [26] P. T. Piiroinen and Yu. A. Kuznetsov. An event-driven method to simulate filippov systems with accurate computing of sliding motions. *ACM Transactions on Mathematical Software*, 34(3):13:1–13:24, 2008.
- [27] T. Putelat, J. H. P. Dawes, and J. R. Willis. On the microphysical foundations of rate-and-state friction. *Journal of the Mechanics and Physics of Solids*, 59(5):1062–1075, 2011.
- [28] D. E. Stewart. Rigid-body dynamics with friction and impact. *SIAM Review*, 42(1):3–39, 2000.
- [29] W. J. Stronge. *Impact mechanics*. Cambridge University Press, 2004.
- [30] D. Takács, G. Orosz, and G. Stépán. Delay effects in shimmy dynamics of wheels with stretched string-like tyres. *Euro. Jnl of Mechanics - A/Solids*, 28(3):516–525, 2009.
- [31] D. Takcs, G. Stpn, and S.J. Hogan. Isolated large amplitude periodic motions of towed rigid wheels. *Nonlinear Dynamics*, 52(1-2):27–34, 2008.
- [32] J. Wojewoda, S. Andrzej, M. Wiercigroch, and T. Kapitaniak. Hysteretic effects of dry friction: modelling and experimental studies. *Phil. Trans. R. Soc. A*, 366:747–765, 2008.